Slag physical property determination: An overview of experimental and computational methods to determine structure, viscosity, electrical conductivity, and thermal conductivity

S. Zaaiman,[1,2] H. Muire, [1,2] and J.H. Zietsman[1,2]

[1]Ex Mente Technologies, Pretoria, South Africa
[2]University Of Pretoria, Pretoria, South Africa

Computational modelling enables those in the pyrometallurgical industry to better understand the materials and processes, improve existing operations, and develop new production technologies. These activities are critical, given the growing challenges of energy availability, raw material quality, and environmental pressure. Importantly, modelling can enable us to do these things faster, with less uncertainty, and with much less risk. However, our ability to accurately calculate slag physical properties such as viscosity, electrical conductivity and thermal conductivity limits how well we can describe high-temperature processes with computational models.

We need better slag property models that we can use in process models and in large multiphysics models of furnaces, kilns, etc., for design, operations, and new technology development. To develop better property models, we need (1) the ability to determine and quantify slag structure since this has a key influence on slag behaviour, and (2) more property data, for more slag compositions, at more temperatures. Such data can be generated with physical measurements and with computational chemistry methods such as molecular dynamics and density functional theory. Both of these are difficult and require specialist equipment and highly skilled personnel. In this paper, we consider the measurement and computational methods that are available for determining the structure, viscosity, electrical conductivity, and thermal conductivity of liquid slags. We present this work to increase the awareness of the importance of slag physical property models to our industry, and of the methods that are available to determine these properties. We also consider whether and how South Africa should invest in establishing a national facility for determining the physical properties of slags and other materials that can assist in extracting more value from our mineral resources.

INTRODUCTION

Slag structure is in its basic form made up of atoms that are chemically bonded to each other. We define slag as a metal and metalloid oxide solution in the liquid phase. Atomic structure of a liquid is difficult to quantify with accuracy. In the context of this paper, slag is defined as a metal and metalloid oxide solution in the liquid state. In industry slag is discussed ambiguously; it is therefore important to clarify what state is referred to in this overview.

Ken Mills has done a lot of work regarding the experimental and computational measurement of slag material properties. Some of his work in Slag Atlas (Allibert and Verein Deutscher Eisenhüttenleute 1995) and the 2011 article Estimating slag properties (Mills, Yuan, and Jones 2011) give the reader an overview of measuring techniques used.

In Treatise on Process Metallurgy, Volume 1: Process Fundamentals silicate slag is defined as a solid within the context of silicate melts (Seetharaman *et al*., 2014). The ionic bond between Si^{4+} and $4O^{-}$ forms a tetrahedron; these tetrahedrons can then be connected to form a polymer chain or Q species. Some cations can break the polymer chain called network breakers (i.e., CaO). Piatak, Parsons, and Seal (2015) defined slag as a primarily silicate-oxide by-product resulting from smelting metallic ore.

The physical properties of slag structures can be measured with experimental or computational techniques. The experimental techniques are done at specialised facilities with expensive equipment. Computational techniques use high-performance computers to perform calculations. Computational techniques are much cheaper than experimental techniques. Data obtained with experimental techniques are used to validate computational techniques. Models are created to estimate the physical properties of slag structures from the experimental data. These models are discussed in Muire, Zaaiman, and Zietsman (2024).

The accurate measurement of the physical properties of slag is important for the pyrometallurgical industry. The data obtained can be used to improve efficiency and lead to the development of new techniques.

The focus is on different measurement techniques used to measure the physical properties of slag. These techniques are split into two sections in this paper: Property Measurement and Computational Methods. The Property Measurement section is further split into Viscosity, Electrical Conductivity, and Thermal Conductivity. Computational methods are split into Molecular Dynamics and Density Functional Theory. This overview gives the reader a general idea of the different available techniques used to measure the physical properties of slag.

Property measurement

The experimental techniques used to measure the physical properties of slag are discussed in this section. The physical properties of interest are structure, viscosity, electrical conductivity and thermal conductivity.

Slag (liquid state) structure is quantified with experimental techniques. The experimental techniques discussed in this section are X-ray diffraction (XRD), Raman spectroscopy, nuclear magnetic resonance (NMR), X-ray absorption near edge structure (XANES), extended X-ray absorption fine structure (EXAFS), and pair distribution function (PDF). Experimental techniques able to measure the liquid phase of the slag are the focus of this section.

The advantages and disadvantages of the various techniques are discussed. Literature examples of slag structure determination for each technique are also given. Table 1 shows the temperature range for each experimental technique discussed.

X-ray Diffraction

XRD works by the principle of X-rays diffracting from atoms in a molecule. The structure of a slag is then obtained from the diffraction pattern. The theoretical basis of Bragg's law is used to determine the diffraction angle of the X-rays (Waseda, Matsubara, and Shinoda, 2011). The absolute molecular structure of the slag can be obtained with a fully crystalline slag sample. The liquid structure is more amorphous than crystal, making it difficult to obtain an absolute molecular structure.

The advantage of XRD is that it is accurate for both crystalline and amorphous samples. The disadvantage is that it does not penetrate the surface of the sample. An important point that should be mentioned is that XRD only gives the species present within a liquid slag.

Raman Spectroscopy

The next experimental method used is Raman spectroscopy which uses the vibrational, rotational, and other low-frequency modes of the atomic structure. The atomic structure is irradiated with monochromatic radiation, usually in the visible light region. The radiation scatter caused by atoms is

then measured by the spectrometer (Colthup, Daly, and Wiberley, 1990). This type of spectroscopy is used to find different structural components of the slag system.

The number of connected Si tetrahedral units (Q^n) was measured by (Jiang, Wu, and You, 2009) at 1473 K in situ for Na_2O-SiO_2. The authors also pointed to the high temperature affecting the intensity of the Raman peaks, which is a considerable drawback of this method.
The advantage of Raman spectroscopy is that it is more sensitive to local short-range order than XRD (Deluca *et al*., 2023).

Nuclear Magnetic Resonance
NMR spectroscopy introduces a magnetic field to the nuclei of the atoms inside the slag that causes the spin of the atoms to change due to the magnetic field. The spin is then detected due to the absorption of the electromagnetic radiation by the specific atoms (Akitt, 1983).

NMR has been used extensively for silicate melt structures. Sukenaga *et al.,* (2006) looked at the effects of oxides on the viscosity of CaO – SiO_2 – Al_2O_3 – (R_2O/RO), where *R* is any cation forming an oxide. The authors used ^{27}Al and ^{29}Si MAS-NMR. One uses an isotope of the desired atom within the compound of interest. The magic angle spinning is when they spin the sample at a magic (special) angle to obtain better resolution.

The biggest benefit of NMR is that the selected compound is detected only without noise from other compounds. The drawback is the large cost and maintenance of the NMR instrument.

X-ray Absorption Near Edge Structure and Extended X-ray Absorption Fine Structure
The exponential decay of energy of photons passing through a sample is the essence of X-ray absorption spectroscopy (XAS). XANES and EXAFS are a subset of the XAS technique. The concept where an X-ray strikes an atom leading to the excitation of an electron leaving an empty hole where the excited electron was, is the basic concept that applies to XANES and EXAFS. The difference in names is from the amount of energy X-rays have where XANES is until approximately 50 eV above the absorption edge and EXAFS is from the XANES region and onwards for approximately 1000 eV. The slag structural information such as bond lengths, bond angles, and bond coordination is obtained using XANES and EXAFS. The XANES region is sensitive to oxidation and geometry while the EXAFS region is sensitive to the radial distribution of electron density from the reference atom leading to the determination of bond length and coordination number (Penner-Hahn, 2003b). The resulting spectrum is the absorbance vs energy, which shows the regions of excitation. Li *et al*., (1993) found the electron transitions of Si in the 3s, 3p, and 3d orbitals with the help of XANES.

The advantage of XANES is its sensitivity to multi-electronic phenomena such as oxidation state, coordination number, and geometry. The drawback is its sensitivity to excited core electrons, which are estimated (Bokhoven and Lamberti, 2015). The disadvantage is that a synchrotron is needed to generate the energy needed for the X-rays needed.

Pair Distribution Function
Lastly, the PDF function is used to obtain an approximate structure when the sample is amorphous or a liquid. PDF is the probability of finding pairs of atoms from a distance *r* of a reference atom. The needed data for PDF is obtained from X-rays, electrons or neutrons fired at the surface of the compound. The PDF function is calculated from the autocorrelation function of the atomic density (Egami and Billinge, 2003).

The biggest advantage is that an approximate structure can be obtained from any type of sample. The biggest drawback of using PDF is when there are bonds with near identical bond lengths it can be difficult to distinguish (Freese, 2018).

Table I. The temperature range for the different experimental techniques and their textbook references

Experimental Technique	Temperature Range (°C)	Reference
XRD	28 - 1973	Waseda, Matsubara, and Shinoda (2011)
Raman Spectroscopy	25 - 2073	Colthup, Daly, and Wiberley (1990)
NMR	25 - 2270	Akitt (1983)
XANES	18 – 2900	Penner-Hahn (2003)
EXAFS	18 - 2900	Penner-Hahn (2003)

Viscosity

Viscosity is the friction when one layer of molecules moves over another layer of molecules. Viscosity is structure and temperature dependent. It is affected by structural factors such as the degree of polymerisation and network modifying cations. There are two types of viscosity, dynamic (absolute) and kinematic. Dynamic viscosity is the ratio of shear stress to velocity gradient defined by Equation (1). The meaning and units for each symbol are given in the Nomenclature section at the end.

$$\mu = \tau \frac{dy}{du} \quad [1]$$

The kinematic viscosity is the ratio of dynamic viscosity to density, defined by Equation (2).

$$\nu = \frac{\mu}{\rho} \quad [2]$$

The methods discussed below measure the dynamic viscosity. There are four main methods with which viscosity is measured, capillary method, falling body method, concentric cylinder method, and oscillating method.

Capillary Method

The capillary method measures the time it takes a liquid to flow through a capillary tube. The capillary method is used only until 1200°C, making it difficult as a universal tool. The reason for this temperature limit is due to the crucible material choices becoming very limited, the capillary material regarding dimensional stability and corrosion resistance. The biggest advantage of this method is that absolute viscosity can be measured and no material calibration is needed.

Falling Body Method

The falling body method measures the time it takes for a body (i.e., sphere) to fall due to gravity or to be dragged upwards through the slag. The viscosity is then calculated using Stokes' law. Absolute viscosity cannot be measured by this method because an apparatus constant is needed that can only be obtained from calibration curves of known viscosities. This technique has been used for glasses and slags.

Concentric Cylinder Method

The concentric cylinder method uses two concentric cylinders with the inner cylinder rotating and the outer cylinder stationary. The inner cylinder is a bob that applies a certain torque and the outer cylinder is a crucible. The limitations of this technique include end effects, wall slip, inertia with secondary flows, eccentricities, and viscous heating (Macosko, 1994).

Oscillating Methods

Viscosity is measured with the oscillating swing of a pendulum within a test liquid at a logarithmic decrease. Oscillating viscometers need to be calibrated first with a reference material with a known viscosity. Relative viscosity values are obtained with the oscillating method. Viscosity in the centipoise range such as CaF_2-based slag is measured with the oscillating method.

Viscometer Methods
Viscometers used in industry plants differ slightly from the ones discussed above. The Herty viscometer uses the length of the slag ribbon formed when poured into the apparatus. Krabiell immersion viscometer works by heating a vessel connected to a rod for 7s in the furnace and then immersing it into the slag for 5s. The mass of the slag that entered the vessel is measured. The incline plane method is similar to the Herty viscometer, but the slag is poured onto an inclined plane and then the length travelled is used to determine slag viscosity.

Experimental errors that could occur when measuring the viscosity with the above-mentioned visometers of a slag include the temperature control and crucible material used. Allibert and Verein Deutscher Eisenhüttenleute. (1995) reported that fewer errors are made when using molybdenum materials.

The most popular technique to measure slag viscosity is the concentric cylinder method due to its ease of operation (Mills, Yuan, and Jones 2011). According to Mills, Yuan, and Jones (2011) the uncertainty is usually 20% for the measurement of slag viscosity with the best techniques only reaching 10% uncertainty. Less than 10% uncertainty is obtained when using correct lab practices. The person doing the viscosity measurements has a substantial influence on the error and accuracy of the results obtained. The repeatability is only as good as the person who performed the measurements. The repeatability of slag measurement should be excellent if the same conditions are used, even when the methods differ. One would incur a large error if the slag does not show Newtonian behaviour (Seetharaman, Mukai, and Sichen 2005).

The various viscosity experimental techniques discussed are from the Slag Atlas (Allibert and Verein Deutscher Eisenhüttenleute., 1995, p. 349-352).

Examples of Viscosity Measurements
Zheng *et al.*, (2014) investigated the CaO – SiO_2 – TiO_2 slag system and determined viscosity using the rotating cylinder method with the Brookfield digital viscometer. The experiment used a Molybdenum crucible and spindle.

Yang *et al.*, (2021) investigated the effect of TiO_2 addition on the CaO – SiO_2 – Al_2O_3 – MgO – TiO_2 – Cr_2O_3 slag system. They used the rotating crucible viscometer (Brookfield viscometer). The crucible and head consist of molybdenum. The viscosity was done in a range of 1420°C to 1500°C.

Chebykin *et al.*, (2017) did viscosity measurements on CaO – Al_2O_3, CaO – SiO_2 and CaO – SiO_2 – Al_2O_3 – MgO blast furnace slag systems using a vibrating finger viscometer. The authors found that the type of finger nose or bob influenced the accuracy of the viscosity. The viscosity was measured up to 1600 °C.

Electrical Conductivity
Electrical conductivity is the ability of a material to conduct an electric current through its atomic structure. The resistance is usually measured as shown in Equation (3). The measurement for electrical conductivity is done by immersing electrodes into the slag and measuring the resistance. There are unfortunately a few problems with this method such as polarisation at the electrode interface, the depth that an electrode is inserted and that slag is not a homogeneous solution (Allibert and Verein Deutscher Eisenhüttenleute., 1995). The different electrode configurations available are central electrode cell, two-electrode cell, ring electrode cell, and four-electrode system.

$$R = \rho_{\text{resis}} \frac{L}{A_{\text{cross}}} = \frac{1}{\sigma} \frac{L}{A_{\text{cross}}} \quad [3]$$

Central Electrode Cell Method
The central electrode cell works by an electrode placed within the slag and the crucible serves as the other electrode. The biggest advantage of this method is the large measuring area of the electrodes; however, the problem with this method is the electrode needs to be placed accurately and the resistance obtained is usually small.

Two Electrode Cell Method
The two-electrode cell uses two electrodes placed within the slag with the resistance measured between these two electrodes. The measuring areas of both electrodes are the same but if the measuring area is too small polarisation can occur. Polarisation at the electrode interface is a concentration gradient that forms which opposes the applied voltage creating another form of resistance that will lead to erroneous readings. Electrical leakage is another occurrence to avoid with two-electrode cells. Electrical leakage occurs when the current moves out of the system into the surroundings.

Ring Electrode Method
The ring electrode cell is a modification of the two-electrode cell where the two electrodes are concentric cylinder-shaped. The biggest advantage of this type of cell is the electrical leakage and stray electrical paths are minimised with a large electrode measuring area. The biggest drawback presented is the different measuring areas for each electrode.

Four Electrode Method
The last method is the four-electrode system where two electrodes are used to apply the current and the other two are used to measure the potential. The four-electrode method uses potentiometric measurements to measure the electrical conductivity. Potentiometric methods determine the resistance by measuring the current and potential from an AC source and applying Ohm's law. This setup largely eliminates the polarisability effects as well as stray electrical currents.

All of these methods to measure electrical conductivity are calibration methods. One has to measure the resistance of a standard liquid first from which the cell constant can be calculated. A problem regularly encountered is the polarisation at the electrode interface. The techniques discussed above work for all slag temperatures. All of the above information is obtained from the Slag Atlas (Allibert and Verein Deutscher Eisenhüttenleute., 1995, p. 557-559).

Calibration-Free Methods
Newly developed techniques to measure electrical conductivity include the two-foil, central electrode, and coaxial cylinder arrangement. These techniques are calibration-free.

The two-foil technique encapsulates the sample in a ceramic crucible sleeve with the other two ends between two foil electrodes that obtain the cell constant with $G = l/A$ where l is the sample thickness and A is the measuring area. The central technique uses two electrodes (central electrode and outer cylinder electrode with alumina ceramics) to isolate the sample. The cell constant is calculated as $G = \ln(r_{out}/r_{in})/2\pi h$ where r_{out} is the radii of the outer sample and r_{in} is the radii of the inner sample and h is the height of the sample. The last measuring technique immerses the sample between two metallic coaxial cylindrical electrodes Zhang *et al.*, (2021). The authors worked in the range of 25 – 1500°C. These new methods discussed are shown in Figure 1.

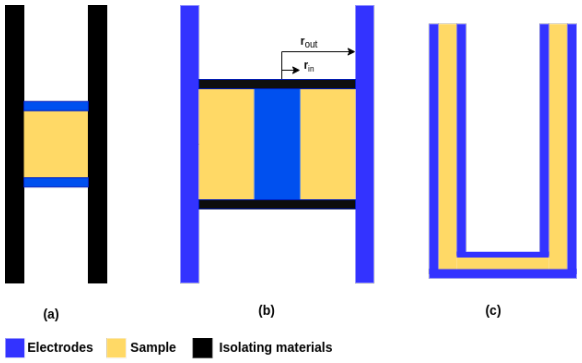

Figure 1. The different experimental setups for measuring electrical conductivity (a) two-foil technique, (b) central electrode technique and (c) coaxial cylinders technique reproduced from Zhang et al. *(2021)*

Thermal Conductivity

Thermal conductivity is the ability of the slag to conduct heat. The transfer of heat occurs by way of vibrational modes. The ability to conduct heat through the slag is influenced by the slag structure and temperature. Thermal conductivity is one of the more difficult properties related to the structure to measure. It is an important physical property that needs to be measured with accuracy.

The measurement of thermal conductivity is divided into three classes: steady-state methods, non-steady state, and transient methods. The effective thermal conductivity (κ_{eff}) is obtained from the steady-state methods. The thermal diffusivity (a_{diff}) is obtained from non-steady state techniques, which can be converted back to effective thermal conductivity. Thermal conductivity is usually measured with heat flux or thermal diffusivity using Equation (4).

$$Q = -\kappa_{\text{eff}}(dT/dx) = \frac{-\kappa_{eff}\Delta T}{d} \quad [4]$$

$$\kappa_{\text{eff}} = a_{\text{diff}} C_p \quad [5]$$

Effective thermal conductivity is used because there are various contributions to thermal conductivity such as radiation, electronic, and lattice phonon conductivity. Radiation conductivity is when the radiant heat energy is transferred through sections of the medium due to the emittance and absorption of photons. Thermal electronic conductivity is the transfer of heat energy through the electronic structure of the slag system. Heat transferred through a medium by way of phonons, which are quanta of energy, is called phonon conduction. The effective thermal conductivity is the sum of these contributions when under optically thick conditions. These conditions are when $ad > 3.5$ where a = absorption coefficient and d = thickness of the sample. The effective thermal conductivity is then given by Equation (6).

$$\kappa_{\text{eff}} + \kappa_{\text{radiation}} + \kappa_{electronic} + \kappa_{\text{phonon}} \quad [6]$$

Steady-State Methods

Steady-state methods aim to ensure temperature is kept constant. The linear heat flow technique uses two disc-shaped samples of the material placed on either side of an electrically heated plate. The temperatures are then monitored on both sides using thermocouples. The whole apparatus is well insulated to prevent heat loss. There are also configurations of this technique that use calorimeters in contact with the sample to measure the heat flow. In the radial heat flow technique the sample is in the shape of a hollow cylinder and then placed between two coaxial cylinders where the centre cylinder is the radial heat source. Temperature is monitored with thermocouples placed on the inside of the two wells. The one drawback with this method is the large isothermal zone required, which is difficult at high temperatures. There is a contribution of radiation conduction when using this method. Convective heat transfer is also present when measuring liquids.

Non-Steady State Methods

The radial wave method uses slag placed in a cylindrical crucible placed in the isothermal zone of the furnace with the thermocouples placed on the geometric axis of the crucible. The crucible is then subjected to a variation in temperature with a thermocouple in the central cylinder used to measure the temperature change. The input and output slag structure has a phase shift caused by the thermal diffusivity. Elliot and co-workers (Fine, Engh, and Elliott, 1976) modified this thermal conductivity measuring instrument by using a periodic variation in temperature that is produced from a wire along the central axis of the crucible with thermocouples measuring the phase shift. There are unfortunately possible errors when obtaining thermal diffusivity this way from convection and radiative heat transfer.

The next non-steady state technique is the modulated beam technique which uses a sample in the form of a disc. The sample is hit with a laser beam which produces a variation of temperature at a constant frequency. The temperature is measured with a sensor at the back of the sample. The phase shift can then be determined by using the input slag phase and the temperature sensor. Schatz and Simmons

(1972) used this method to determine both the thermal diffusivity and the extinction coefficient (molar absorption coefficient). Convection is again another source of error that can arise in liquids.

Transient Methods
The transient of the temperature-time curve is measured for a short duration with the input of energy for these methods. The laser pulse method uses a disc of dimensions 10 mm to 15 mm with a laser pulse directed on one side of the disc with the temperature monitored at the other side. The temperature transient reaches a maximum that can be used to calculate the thermal diffusivity using Equation (7)

$$a_{\text{diff}} = \frac{1.37d^2}{\pi^2 t_{0.5}} \quad [7]$$

The laser pulse method can also be used for the liquid phase where a platinum disc is on top of the liquid sample with the temperature constantly measured. The radiation (photon) conductivity and lattice phonon conductivity can also be obtained with numerical manipulation.

The last method to measure thermal conductivity is the line source method (transient hot wire method) which uses a long thin wire. A current is applied to the wire causing the wire to act both as a heat source and resistance thermometer that measures the temperature of the wire continuously. The thermal conductivity is then calculated from the Equation (8):

$$\Delta T = \frac{q}{4\pi} ln \frac{4at}{r^2 e^{\gamma}} \quad [8]$$

The thermal conductivity can be calculated from the slope ($1/k$) as well with the δT ln time graph. The advantages of this method are that any convection occurring will result in a departure from linear behaviour and radiation conductivity is very low in this method. The techniques discussed are from the Slag Atlas (Allibert and Verein Deutscher Eisenhüttenleute., 1995, p. 591-594).

Computational Methods
Different computational methods used to find the structure and other thermodynamic properties of slag are focused on next. The two main techniques used are discussed and examples are given where researchers used them.

The two most common techniques used are molecular dynamics (MD) and density functional theory (DFT). Classical MD is a bit simpler than DFT due to quantum mechanical calculations being omitted to improve computation time. Notably, both these techniques require a large amount of computational power, much more than found on an average workstation computer.

Figure 2 shows a sodium alumino-silicate hydrate (N-A-S-H) gel. The system consists primarily of silicon and aluminium tetrahedral. Figure 3 shows a Cu – Au alloy with the radial distribution function and the number of structural units present. These two figures are purely examples of what MD studies look like, they are not discussed further because they are not in the scope of this article.

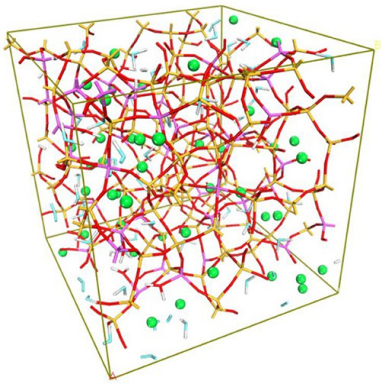

Figure 2. The atomic model for the structure of N-A-S-H that consists of a three-dimensional aluminosilicate skeleton filled with sodium and water molecules using molecular dynamics. Silicon and aluminium species are predominantly tetrahedral. Reproduced from (Wan, Yuan, and Zhang, 2020) CC BY 4.0.

Molecular Dynamics

MD uses classical mechanics to model the interactions between atoms without taking any quantum mechanical interactions into account. In its simplest form, it is calculated with Newton's second law $F = ma$ therefore only the velocities and atomic positions are computed. MD uses a potential function to model the interactions taking place within the system. The potential function is the restricting part of MD because the atoms can only behave within the confines of this potential function. The application largely determines the potential function that will be used. Furthermore, experimental data is sometimes incorporated into the function and used as the starting point.

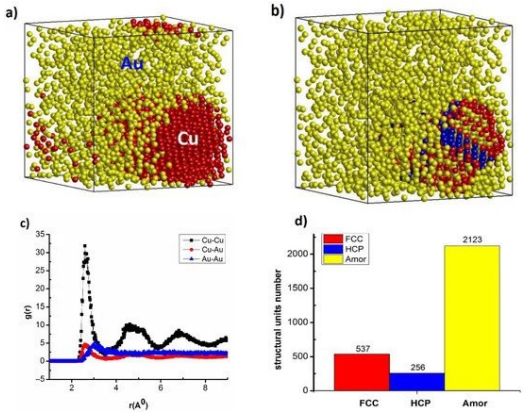

Figure 3. The (a) initial conditions for the MD simulation of the Cu-Au alloy, (b) the resulting mixture of Cu and Au atoms, (c) the radial distribution function, and (d) number of structural units. The heating rate is 4 × 10^{12} K s^{-1} for 3 fs starting from 300 K. Reproduced from (Quoc et al.*, 2022) CC BY 4.0.*

However, chemical reactions can be modelled with MD to some degree. One can start from the ground up and give no input for the model by using *ab initio* molecular dynamics (AIMD). The potential functions used in AIMD utilise the electronic structure (position and movement of electrons) of the atoms to model the formation and breaking of bonding. Although these potential functions use the electronic structure, it does not match the degree and precision of Schrödinger-equation solving calculations (i.e., quantum mechanical calculations). MD is used for large simulations of 1000 atoms and upward-sized systems. The simulation is usually done for a femtosecond (1 × 10^{15} s) and the results are then averaged over the specified time.

A simple way to interpret molecular dynamics simulations is to think of balls of different sizes getting mixed in a container interacting and bouncing against, each other after which the desired property can be calculated. AIMD can be explained by the same analogy but this time the balls are connected to move

as a single connected unit where the connection between the balls is a chemical bond. Note that the electrons are the glue that keep all the nuclei together.

Equilibrium molecular dynamics (EMD) simulate a chemical system for a certain time period to reach equilibrium conditions. The Green-Kubo method uses time integrals of time correlation functions to express diffusion, thermal conductivity, and viscosity coefficients as examples. The method utilises linear response theory in statistical mechanics to obtain an equilibrium condition for the system.

Potential functions
The various potential functions used for MD are discussed next. The mathematical form of the potential function is shown to give a comprehensive explanation of the function. Commonly used potential functions are Born-Mayer (BM), Lennard-Jones (L-J), and Embedded Atom Model (EAM).

Born-Mayer
The BM function (Equation (9)) is a potential function used to describe ions in an ionic crystal as well as used for silicate and aluminate systems. Ionic bonds form when there is a significant difference in electronegativities leading to a transfer of electrons. The BM model is a pair potential that has an attractive and repulsive term meaning between two atoms.

$$\phi_{\mathrm{BM}}(r) = \frac{z_i z_j e^2}{4\pi\epsilon|r|} + A_{ij}\left(1 + \frac{z_i}{n_i}\frac{z_j}{n_j}\right) e^{\sigma_i + \sigma_j - r/\rho_{ij}} \quad [9]$$

Lennard-Jones
The L-J potential function (Equation (10)) is a pair potential function that models the weak Van der Waals forces between atoms. The L-J potential function works very well to model noble gases. The bond energies and bond lengths are then obtained.

$$V_{\mathrm{LJ}}(r) = 4\epsilon\left[\left(\frac{\sigma_{exp}}{r}\right)^{12} - \left(\frac{\sigma_{exp}}{r}\right)^{6}\right] \quad [10]$$

The sixth power term is the attractive term (dipole-dipole interactions) which is assumed to decay with distance and the twelfth power term is the repulsive term (Pauli exclusion principle).

Embedded Atom Model
The EAM potential function (Equation (11)) was developed to explain atomic interactions in metals. In the EAM the metal is described as a collection of positive charges immersed in a sea of electrons. The total energy can then be obtained from the energy gained by embedding an ion in an electron sea and the repulsion between ions.

$$E_{\mathrm{tot}} = \sum_i F(\rho_i) + \frac{1}{2}\sum_{i,j(i\neq j)} \phi_{ij}(R_{ij}) \quad [11]$$

The electron density of the 'sea of electrons' is given by Equation (12).

$$\rho_i = \sum_{j\neq i} \rho_j^a(R_{ij}) \quad [12]$$

Stillinger-Weber
The last potential considered is the Stillinger-Weber (SW) potential function. The SW potential function (Equation (13)) is used to model covalent bonds. Covalent bonds form when there is a small difference in electronegativities between atoms. Covalent bonds are more complex to model because the electrons are delocalised between the two atoms resulting in forces between electrons and nuclei-electrons to become relevant. The model has a pair potential and an angle-dependent three-body term.

$$V_{\mathrm{SW}} = \frac{1}{2}\sum_{ij} \phi(r_{ij}) + \sum_{ijk} g(r_{ij}) g(r_{ik}) \left(\cos\theta_{ijk} + \frac{1}{3}\right)^2 \quad [13]$$

The Stillinger-Weber function works well with $\cos\theta_{ij\bar{k}} = \frac{1}{3}$ which is the angle for a tetrahedral structure. $g(r)$ is a function that decays with a distance where the cutoff is between the first and second nearest neighbours.
MD is performed with restrictions to increase the computational speed or to investigate specific properties of a system. These restrictions consist of ensembles: NVE, NVT, and NPT. The information on MD is adapted from the book chapters Introduction to Molecular Dynamics by Schneider, Sharma and Rai in the book Computational Many-Particle Physics (Schneider, Sharma, and Rai, 2008) and Bonding Energy Models by Adams in the book Encyclopedia of Materials: Science and Technology (Adams, 2001).

Density Functional Theory
DFT is a fundamental modelling tool because it uses quantum mechanics instead of classical mechanics to find the energy and thermodynamic values of the system. Hohenberg-Kohn and Kohn-Sham developed the theory in the 1960s. DFT determines the electron density (electrons per unit volume) to solve the Schrödinger equation instead of the many-electron approach. The electronic structure is solved for the chemical system meaning the way electrons move and interact within the structure. The exchange and correlation behaviour of electrons is accounted for in DFT. This refers to electrons replacing each other in orbitals and repulsing each other as they move through the chemical system. Electrons are both a particle and a wave; both of these behaviours need to be accounted for to prevent a partial description of the chemical system from arising. The big attraction of using DFT is the accuracy obtained for the computational time taken which is better than MD. DFT has also been used in combination with MD where an MD simulation is done and at chosen steps the structure is energy-optimised using DFT to keep using the lowest energy conformer as the simulation continues.

A higher level of detail for molecular systems is attainable with higher levels of theory such as Møller-Plesset Second-Order Perturbation Theory (MP2) and Coupled Cluster Singles and Doubles (CCSD). These methods are more accurate but are computationally expensive. CCSD with single and double substitutions is the golden standard but is computationally expensive to an extreme degree. These two methods have not been used for slag systems to our knowledge.

For a basic understanding of DFT one can imagine a molecular system that consists of three arbitrary atoms, each with several electrons. DFT is based on the Born-Oppenheimer approximation, which states that the nuclei are stationary and the electrons are moving due to the large difference in velocities of the electrons and the nuclei. The total energy is calculated as kinetic energy plus potential energy. Both the electrons and nucleus need to be accounted for in the energy calculation. The total energy is $E_k^n + E_k^e + E_p^{e-e} + E_p^{e-n}$ then: E_k is kinetic energy, E_p potential energy, subscript n is the nucleus and e is the electron. The kinetic energy of the nucleus is zero because it is assumed to be stationary. When calculating the energy terms here both the classical electrostatic interactions and the quantum effects are taken into account. Quantum effects are the forces between electrons other than classical electrostatic interactions. The 3-atom system is then optimised by moving the atoms around and calculating the energy values for the different points in space until the lowest energy system is found.

These interactions between electrons and electron-nucleus make up the electronic energy which is the total energy of the system. The only shortcoming of DFT is from the quantum effects between electrons as these cannot be calculated exactly; however, they are approximated reasonably well. If the quantum effects were exact then DFT would have been 100% accurate. The DFT calculation is done at 0 K to obtain the ground state of the molecular system. DFT can be done at higher temperatures but this requires modifications which involve much more detail regarding DFT and the basis set that is beyond the scope of this article.

Property Computation
Slag structure, viscosity, electrical conductivity, and thermal conductivity are investigated with computational methods. Examples are given where researchers investigated these thermophysical properties. The researchers compared their findings to experimental data to ensure their data are accurate. This section serves as a proof that computational techniques can be used and should be

considered more readily in industry.

Structure
Sun *et al.*, (2022) investigated the binary slag CaO – Al_2O_3 with deep potential molecular dynamics (DPMD) based on AIMD data. The deep potential is a neural network that needs a dataset that covers the entire range of the compositions that exist for the slag system. The authors performed AIMD calculations for a wide range of CaO mole fractions. The calculation was done with the Perdew-Burke-Ernzerhof (PBE) Generalised Gradient Approximation (GGA) exchange-correlation functional and projector augmented wave (PAW) method to reach equilibrium at 1900 K. Furthermore, the authors used the DeePMD-kit package for the deep learning process. After training the DPMD performed calculations with Large Scale Atomic/Molecular Massively Parallel Simulator (LAMMPS) for approximately 5000 atoms.

The authors found that in the slag system, CaO dissociates into Ca^{2+} and O^{2-} resulting in various $[AlO_n]^{-b}$ species as the CaO molar fraction is in the range of 0.50 and 0.70. The increase in X_{CaO} causes the diffusion coefficients of Al and O to slightly decrease. The authors successfully combined AIMD and DPMD to investigate the structure of the CaO – Al_2O_3 slag system.

Jiang *et al.*, (2018) investigated the effect of MgO/Al_2O_3 ratio on the Cao – MgO – Al_2O_3 – SiO_2 using MD within the LAMMPS package with the CMAS94 model (Matsui 1994). The system mainly consisted of SiO_4^{4-} and AlO_4^{5} tetrahedrons. When the MgO/Al_2O_3 ratio increased the degree of polymerisation decreased. The diffusion coefficients of the Si^{4+} were the lowest due to the strong bond it forms with O and the highest was Mg^{2+}. The smaller radius for Mg^{2+} caused the diffusion to be higher than Ca^{2+}. The diffusion coefficient increased when the Al_2O_3 content increased. However, when the MgO/Al_2O_3 ratio is 0.4 this is not the case because there is an insufficient amount of network modifiers leading to a slowly decreasing degree of polymerisation. An increase in the Al_2O_3 content leads to a decrease in the viscosity which correlates with experimental results. When Al_2O_3 content increases the SiO_4^{4-} content decreases ultimately leading to a less stable overall structure.

Viscosity
He *et al.*, (2019) investigated the CaO – SiO_2 – CaF_2 slag system to determine the effect CaF_2 has on structure and viscosity of the slag. The Born-Mayer-Huggins (BMH) pair-wise potential function was used.

Interestingly, CaF_2 did not have a significant effect on the depolymerisation and viscosity. The CaF_2 caused some Si atoms to form a tetrahedron with F instead of O. The CaF_2 acts as a network modifier causing the melting temperature to decrease. The increase in basicity caused an increase in depolymerisation leading to a decrease in viscosity. The MD simulation viscosity values closely matched those obtained from FactSage (Bale *et al.*, 2016).

Kim and Park (2019) investigated the viscosity of TiO_2 – FeO – Na_2O using the Buckingham potential in the LAMMPS package. The simulation contained 8000 atoms with only Fe^{2+} present as the iron species. The authors found that the addition of Na_2O resulted in a lower liquidus temperature and viscosity of the slag at 6 mol%. The radial distribution function (RDF) showed the presence of a TiO_6 octahedral network. The Ti atom had the slowest diffusion due to the presence of a TiO_6 octahedral network structure and thus the biggest factor for viscosity. Higher TiO_2 concentrations led to higher viscosity in the FeO – TiO_2 slag system. The octahedral network becomes depolymerised when more FeO is added to the FeO – TiO_2 slag system. The experimental viscosities were in excellent agreement with the MD simulations.

Electrical Conductivity
Mongalo, Lopis, and Venter (2016) investigated the structural properties and electrical conductivity of the CaO – MgO – Al_2O_3 – SiO_2 slag system with MD. The Morse potential was used to model interactions between the atoms using the vibrational and dissociation energies. The Morse potential is similar to an anharmonic oscillator. The MD simulations had between 2000 and 2150 atoms.

The number of bridging oxygens showed that both tetrahedral SiO_4^{4-} and AlO_4^{5-} are present using the Q^n distribution. The electrical conductivities obtained were in good agreement with the experimental values. The authors noted that if electrical conductivity values are calculated indirectly, caution should be used. Lastly, they found a reasonable agreement between Zachariasen's Random Network Model and the simulation at low basicity with deviation when network modifying cations increased.

Thermal Conductivity

Wang *et al.*, (2020b) studied the thermal conductivity of the CaO – Al_2O_3 – SiO_2 using EMD. The simulations were done using the BMH potential function and contained approximately 1000 atoms. The study was performed with EMD by using the Green-Kubo method within the LAMMPS package.

The thermal conductivity obtained for the CaO – Al_2O_3 – SiO_2 slag system was in good agreement with the experimentally obtained values. The authors found a direct correlation between the bridging oxygens and thermal conductivity where both decreased when slag systems that consist of similar CaO/SiO_2 ratios were compared. The combined network of Al– O and Si – O leads to a higher thermal conductivity compared to a simple Si – O network. Lastly, the potential function and a reasonable initial structure are the most important for the accuracy of the thermal conductivity.

Wang *et al.*, (2020a) investigated the effect of temperature on CaO – SiO_2 – Al_2O_3 slags. The MD simulation was performed using the BMH interatomic potential within the LAMMPS package and consisted of 1000 atoms.

The Green-Kubo method was used for the EMD. The thermal conductivity is calculated with the autocorrelation function using the heat current data. Ca^{2+} has a significant effect on the configurational entropy due to its effect on the angles of the tetrahedrals in the aluminosilicate chain. Increased ratio of CaO/Al_2O_3 and CaO/SiO_2 caused depolymerisation to take place. The authors found that an increase in temperature led to an increase in the heat capacity equating to an increase in the thermal conductivity. The large benefit of the EMD is the fact that it can simulate the heat transfer process accurately. Additionally, the authors employed partial least squares regression to try and find the most important contribution to thermal conductivity using machine learning. The conclusions from the machine learning investigation are that the most important factor is temperature more so than the CaO/Al_2O_3 and CaO/SiO_2 ratios.

There are very few investigations done with only DFT calculations on slag systems. This is due to the computational time taken with such large systems. MD has proven to be sufficient with material physical properties but is still limited. AIMD is very effective due to the incorporation of quantum mechanics with a little less precision than DFT but faster computation time. The study by (He and Wang, 2023) discussed below uses DFT but not on the material physical properties as discussed above. The reason for this inclusion is to show the potential of DFT in slag systems.

He and Wang (2023) investigated the interfacial properties between an Mn-based slag and an S-containing liquid metal. The calculations were performed via the Vienna *ab initio* Simulation Package (VASP) with the PAW method and PBE exchange-correlation functional. The PAW basis set is an electronic structure calculation method that generalises both the pseudopotential method and the Linear Augmented-Plane Wave (LAPW) method in a natural manner. The computational time is enhanced with this method. The PBE functional is a GGA-type functional to model the exchange-correlation behaviour of electrons.

The combination of the experimental and computational results showed that bridging O atoms decreased and the number of non-bridging O atoms increased as the metal-slag surface etching depth increased. The higher basicity levels cause the diffusion of the S to increase leading to a decrease in FeS at the interface. The proposed reactions occurring at the interface are an oxidation reaction of Fe with Mn/Si in the slag and an exchange reaction between S and O leading to the dissolution of S. The S forms then a stable sulfide with metal elements such as Mn and Ca as well as aggregate at the interface.

Table II. Summary of strengths and weaknesses of molecular dynamics and density functional theory

Computational Method	Strength	Weakness
DFT	Calculates from first principles Great accuracy	Computationally expensive
MD	Computationally efficient Can model 1000+ atom systems	Requires appropriate potential function

Measuring Facilities

The different facilities available to measure the physical properties of a slag are shown in Table 2. These facilities include all the experimental techniques discussed in Property Measurement and computational tools discussed in Property Computation. The facilities are located all over the world and are not limited to the ones shown in Table 2. The facilities are shown to give an idea of where one can go to measure the physical properties of slags.

Table III. Some of the available facilities to measure the physical properties of slags

Experimental Technique	Available Facilities	Country of Facilities
Slag Structure Determination		
XRD	University of Pretoria, University of Cape Town, Wits University	SA
NMR	University of Pretoria, University of Cape Town, University of Johannesburg,	SA
Raman Spectroscopy	University of Stellenbosch	SA
XANES	University of Pretoria, University of Johannesburg, University of Cape Town,	USA, UK
EXFAS	Anatech	India, UK
	SLAC National Laboratory, Diamond Light Source	
	RRCAT, Synchrotron Radiation Source	
Thermal Conductivity		
LFA	Karlsruhe Institute of Technology (KIT), Infinta lab, Institute of Plasma Research	Germany, USA, India
THWM	University of Western Australia, University Complutense of Madrid	Australia, Spain
Electrical Conductivity		
2 electrode	CSIRO	Australia
4 electrode	McMaster University	Canada
CSLM	Katholieke Universiteit Leuven	Belgium
Molecular Simulation Software		
Molecular Dynamics Density Functional Theory	LAMMPS, GROMACS, NAMD, HOOMD-blue, OpenMM, ESPResSo, DL_POLY, GULP, CP2K, AMBER, NWCHEM, Tinker, GROMOS GAMESS, Gaussian, NWChem, ADF, CP2K, Q-Chem, TURBOMOLE, MOLCAS, MOLPRO, PSI4, MRCC, DIRAC, DALTON, deMon2k, AcesIII, BAGEL, CFOUR, LSDALTON, OpenMolcas, ORCA	

National Facility

One of the most important resources needed today is a facility in South Africa for the experimental and computational measuring of slag systems. The only way to move forward and make significant strides with these complex systems is to work together. There are a few experimental techniques available at Mintek in Randburg and computational resources at the Centre for High-Performance Computing in Cape Town. There are also experimental techniques available at the Council of Scientific and Industrial Research. All of these facilities together can solve difficult problems related to slags. There exists a material properties consortium Pyro-MPP that collaborates to solve problems related to the material properties of slags.

CONCLUSION

The experimental techniques to determine slag structure serve as a toolbox for the experimental researcher to use. The experimental researcher must choose the correct tool for the job. The best result is usually achieved when more than one experimental technique is used for a slag system. Slag structure is difficult to measure with accuracy in the liquid phase. Viscosity is measured with reasonable accuracy but the high-temperature viscosity is difficult to measure. Thermal conductivity and electrical conductivity are difficult properties to measure without incurring some form of an error. Newer methods are necessary for both of these material physical properties.

Computational methods are a similar situation where they serve different purposes but there are some drawbacks due to the complexity of chemical systems. Computational methods such as the AIMD and EMD can estimate these material physical properties with high accuracy. There are limited studies done purely with DFT on slag systems. The structure, viscosity, electrical conductivity, and thermal conductivity have all been quantified by MD with reasonable accuracy. There are many computational tools available for the computational researcher to obtain a good estimate of the material physical properties.

A national facility is a collaboration that is necessary for the future. The biggest benefit of such a facility is the sharing of knowledge and resources. The facility will be able to push the boundaries of slag research and provide a platform for the next generation of researchers to learn and grow.

NOMENCLATURE

Slag Structural Property Quantities

Quantity	Description
Q^n	number of Si tetrahedral units bonded to the specific Si tetrahedral (mol. mol^{-1})

Viscosity Property Quantities

Quantity	Description
μ	dynamic viscosity (Pa s)
τ	shear stress (Pa)
ν	kinematic viscosity (m^2 s^{-1})
ρ	density (kg m^{-3})

Electrical Conductivity Property Quantities

Quantity	Description
σ	electrical conductivity (S m^{-1} or Ω−1 m^{-1})
ρ_{resis}	electrical resistivity (Ω ·
R	m) electrical resistance (Ω)
A_{cross}	cross-sectional area (m^2)
L	distance current travels (m)

Thermal Conductivity Property Quantities

Quantity	Description
κ_{eff}	thermal conductivity (W m^{-1} K^{-1})
κ_{phonon}	phonon thermal conduction (W m^{-1} K^{-1})
$\kappa_{radiation}$	radiative thermal conduction (W m^{-1} K^{-1})
$\kappa_{electronic}$	electronic thermal conduction (W m^{-1} K^{-1})
Q	heat flux (W m^{-2})
a_{eff}	thermal diffusivity (m^2 s^{-1})
C_p	heat capacity (J mol^{-1} K^{-1})
ρ	density (g cm^{-3})
a	absorption coefficient (m^{-1})
d	thickness of sample (m)
$t_{0.5}$	half the time it takes to reach the transient temperature max (s)
q	heat per unit length (W m^{-1})
γ	Eulers constant

Molecular Dynamics Property Quantities

Quantity	Description
z	atomic charge
n_i	the number of valence electrons of the ion
σ_i	size of an ion
ρ_{ij}	softness of electron cloud
r	distance between two atoms
ϵ	experimental fitting parameters
σ_{exp}	experimental fitting parameters
$F(\rho_i)$	embedding energy needed to embed an ion in the electron sea
$\phi_{ij}(R_{ij})$	the short-range electrostatic interaction between ions with the distance between ions denoted by R.
$\rho^a_j(R_{ij})$	is the electron density contribution of atom j
θ_{ijk}	angle formed by the *ij* bond and the *ik* bond

REFERENCES

Adams, J.B. (2001). "Bonding Energy Models". In: Encyclopedia of Materials: Science and Technology. Ed. by K.H. Jurgen Buschow, Robert W. Cahn, Merton C. Flemings, Bernhard Ilschner, Edward J. Kramer, Subhash Mahajan, and Patrick Veyssière. Oxford: Elsevier, pp. 763–767. ISBN: 978-0-08-043152-9. DOI: 10.1016/B0-08-043152-6/00146-7.

Akitt, J. W. (1983). NMR and Chemistry : An Introduction to the Fourier Transform-Multinuclear Era. 2nd ed. Science Paperbacks ; 185. London ; Chapman and Hall. Chap. xiii, 263 pages. ISBN: 0-412-24010-69780-412-24010-2 0-412-24020-3 978-0-412-24020-1.

Allibert, M. and Verein Deutscher Eisenhüttenleute. (1995). Slag Atlas. 2nd ed. Düsseldorf: Verlag Stahleisen. Chap. xviii, 616 pages. ISBN: 3-514-00457-9 978-3-514-00457-3.

Bale, C.W. et al. (Sept. 2016). "FactSage Thermochemical Software and Databases, 2010–2016". In: Calphad 54, pp. 35–53. ISSN: 03645916. DOI: 10.1016/j.calphad.2016.05.002. (Visited on 09/05/2020).

Bokhoven, Jeroen A. van and Carlo Lamberti, eds. (2015). X-Ray Absorption and X-ray Emission Spectroscopy: Theory and Applications. Chichester, West Sussex: John Wiley & Sons, Inc. ISBN: 978-1-118 84423-6.

Chebykin, Dmitry, Hans-Peter Heller, Tobias Dubberstein, Iurii Korobeinikov, and Olena Volkova (2017). "Viscosity Measurement of Slags Using Rotating Bob and Vibrating Finger Viscometer". In: ISIJ International 57.8, pp. 1319–1326. ISSN: 0915-1559, 1347-5460. DOI: 10.2355/isijinternational.ISIJINT-2016-580. (Visited on 09/26/2023).

Colthup, Norman B., Lawrence H. Daly, and Stephen E. Wiberley (1990). Introduction to Infrared and Raman Spectroscopy. 3rd ed. Boston: Academic Press. Chap. xii, 547 pages. ISBN: 0-12-182554-X978-0-12-182554-6.

Deluca, Marco, Hailong Hu, Maxim N. Popov, Jürgen Spitaler, and Thomas Dieing (Oct. 2023). "Advantages and Developments of Raman Spectroscopy for Electroceramics". In: Communications Materials 4.1, p. 78. ISSN: 2662-4443. DOI: 10.1038/s43246-023-00400-4. (Visited on 11/20/2023).

Downes, Andrew and Alistair Elfick (Mar. 2010). "Raman Spectroscopy and Related Techniques in Biomedicine". In: Sensors 10.3, pp. 1871–1889. ISSN: 1424-8220. DOI: 10.3390/s100301871. (Visited on 02/28/2024).

Egami, Takeshi and S. J. L. Billinge (2003). Underneath the Bragg Peaks: Structural Analysis of Complex Materials. Pergamon Materials Series v. 7. Kiddington, Oxford, UK Boston: Pergamon. ISBN: 978-0-08-042698-3.

Fine, H. Alan, T. Engh, and John F. Elliott (June 1976). "Measurement of the Thermal Diffusivity of Liquid Oxides and Metallurgical Slags". In: Metallurgical Transactions B 7.2, pp. 277–285. ISSN: 2379-0229. DOI: 10.1007/BF02654927.

Freese, Brett (2018). "Exploring Extended X-ray Absorption Spectroscopy and Pair-Distribution Function Methods in Amorphous Semiconductors". PhD thesis. DePaul university.

He, Shengping, Sai Wang, Boran Jia, Min Li, Qiangqiang Wang, and Qian Wang (June 2019). "Molecular Dynamics Simulation of the Structure and Properties of CaO-SiO_2-CaF_2 Slag Systems". In: Metallurgical and Materials Transactions B 50.3, pp. 1503–1513. ISSN: 1073-5615, 1543-1916. DOI: 10 . 1007 / s11663 - 019 - 01547 - 7. (Visited on 10/30/2023).

He, Xiaobo and Lijun Wang (June 2023). "Insights into Interfacial Structure of Slag–Metal Interface During Desulfurization Through XPS and DFT Simulations". In: Metallurgical and Materials Transactions B 54.3, pp. 1043–1055. ISSN: 1073-5615, 1543-1916. DOI: 10.1007/s11663-023-02759-8. (Visited on 10/04/2023).

Inaba, Katsuhiko, Shintaro Kobayashi, Kenichi Uehara, Akira Okada, Sanapa Lakshmi Reddy, and Tamio Endo (2013).

"High Resolution X-Ray Diffraction Analyses of (La,Sr)MnO_3/ZnO/Sapphire(0001) Double Heteroepitaxial Films". In: Advances in Materials Physics and Chemistry 03.01, pp. 72–89. ISSN: 2162-531X, 2162-5328. DOI: 10.4236/ampc.2013.31A010. (Visited on 02/28/2024).

Jiang, Chunhe, Kejiang Li, Jianliang Zhang, Qinghua Qin, Zhengjian Liu, Minmin Sun, Ziming Wang, and Wang Liang (Dec. 2018). "Effect of MgO/Al2O3 Ratio on the Structure and Properties of Blast Furnace Slags: A Molecular Dynamics Simulation". In: Journal of Non-Crystalline Solids 502, pp. 76–82. ISSN: 00223093. DOI: 10.1016/j.jnoncrysol.2018.06.043. (Visited on 10/31/2023).

Jiang, Guo-Chang, Yong-Quan Wu, and Jing-Lin You (2009). "THE HIGH TEMPERATURE RAMAN SPECTROSCOPY AND ION CLUSTER THEORY FOR METALLURGICAL SLAG AND MAGMA". In: Molten 2009 : proceedings of the VIII International Conference on Molten Slags, Fluxes & Salts.

Kim, Youngjae and Hyunsik Park (Nov. 2019). "Estimation of TiO2-FeO-Na2O Slag Viscosity through Molecular Dynamics Simulations for an Energy Efficient Ilmenite Smelting Process". In: Scientific Reports 9.1, p. 17338. ISSN: 2045-2322. DOI: 10.1038/s41598-019-53961-1. (Visited on 10/03/2023).

Li, Dien, G M Bancroft', X H Feng, K H Tan, and B X Yang (1993). "HIGH-RESOLUTION SI K- AND $L_{2,3}$-EDGE XANES OF □-QUARTZ AND STISHOVITE". In: Solid State Communications 87.7, pp. 613–617.

Macosko, Christopher W. (1994). Rheology : Principles, Measurements, and Applications. Advances in Interfacial Engineering Series. New York, NY: VCH New York, NY. Chap. XVIII, 550 p. : il., gràf. ISBN: 1-56081-579-5 978-1-56081-579-2 0-471-18575-2 978-0-471-18575-8.

Mills, K.C., L. Yuan, and R.T. Jones (2011). "Estimating the Physical Properties of Slags". In: Journal of the

Southern African Institute of Mining and Metallurgy 111, pp. 649–658. (Visited on 01/21/2021).

Mongalo, Lehlohonolo, Anton S. Lopis, and Gerhard A. Venter (Nov. 2016). "Molecular Dynamics Simulations of the Structural Properties and Electrical Conductivities of CaO–MgO–Al2O3–SiO2 Melts". In: Journal of Non-Crystalline Solids 452, pp. 194–202. ISSN: 00223093. DOI: 10.1016/j.jnoncrysol.2016.08.042. (Visited on 12/07/2020).

Muire, H., S. Zaaiman, and J.H. Zietsman (2024). "Slag physical property models and data: A review of structure, viscosity, electrical conductivity, and thermal conductivity".

Mysen, Bjorn and P Richet (2005). Silicate Glasses and Melts: Properties and Structure. Elsevier.

Penner-Hahn, James E (2003a). "X-Ray Absorption Spectroscopy". In: Comprehensive Coordination Chemistry II , pp. 159–186.

Ed. by Jon A. McCleverty and Thomas J. Meyer. Oxford: Pergamon, pp. 159–186. ISBN: 978-0-08-043748-4. DOI: 10.1016/B0-08-043748-6/01063-X.

Piatak, Nadine M., Michael B. Parsons, and Robert R. Seal (June 2015). "Characteristics and Environmental Aspects of Slag: A Review". In: Applied Geochemistry 57, pp. 236–266. ISSN: 08832927. DOI: 10.1016/j.apgeochem.2014.04.009. (Visited on 02/19/2024).

Quoc, Tuan Tran, Van Cao Long, Ştefan Ţălu, and Dung Nguyen Trong (Jan. 2022). "Molecular Dynamics Study on the Crystallization Process of Cubic Cu–Au Alloy". In: Applied Sciences 12.3, p. 946. ISSN: 2076-3417. DOI: 10.3390/app12030946. (Visited on 10/24/2023).

Schatz, John F. and Gene Simmons (1972). "Thermal Conductivity of Earth Materials at High Temperatures". In: Journal of Geophysical Research (1896-1977) 77.35, pp. 6966–6983. DOI: 10.1029/JB077i035p06966. eprint: https://agupubs.onlinelibrary.wiley.com/doi/pdf/10.1029/JB077i035p06966.

Schneider, Ralf, Amit Raj Sharma, and Abha Rai (2008). "Introduction to Molecular Dynamics". In: Computational Many-Particle Physics. Ed. by H. Fehske, R. Schneider, and A. Weiße. Berlin, Heidelberg: Springer Berlin Heidelberg, pp. 3–40. ISBN: 978-3-540-74686-7. DOI: 10.1007/978-3-540-74686-7_1.

Seetharaman, Seshadri., Alex 1936 McLean, Roderick I. L. Guthrie, and Seetharaman. Sridhar (2014). Treatise on Process Metallurgy. Vol. 1. Kidlington, Oxford, U.K. ; Elsevier. ISBN: 978-0-08-096987-9 0-08-096987-9 978-0-08-096985-5 0-08-096985-2 978-0-08-096989-3 0-08-096989-5.

Seetharaman, Seshadri, Kusuhiro Mukai, and Du Sichen (Apr. 2005). "Viscosities of Slags - an Overview". In: steel research international 76.4, pp. 267–278. ISSN: 1611-3683, 1869-344X. DOI: 10.1002/srin.200506008. (Visitedon 02/15/2024).

Sukenaga, Souhei, Noritaka Saito, Kiyoshi Kawakami, and Kunihiko Nakashima (2006). "Viscosities of CaO-SiO_2-Al_2O_3-(R_2O or RO) Melts". In: ISIJ International 46.3, pp. 352–358. ISSN: 0915-1559, 1347-5460. DOI: 10.2355/isijinternational.46.352. url: http://www.jstage.jst.go.jp/article/isijinternational/46/3/46_3_352/_article (visited on 06/21/2023).

Sun, Yuhan, Min Tan, Tao Li, Junguo Li, and Bo Shang (May 2022). “Study on the Structural Properties of Refining Slags by Molecular Dynamics with Deep Learning Potential”. In: Journal of Molecular Liquids 353, p. 118787. ISSN: 01677322. DOI: 10.1016/j.molliq.2022.118787. (Visited on 10/30/2023).

Wan, Hongyan, Liqun Yuan, and Yu Zhang (Mar. 2020). “Insight Into the Leaching of Sodium Alumino-Silicate Hydrate (N-A-S-H) Gel: A Molecular Dynamics Study”. In: Frontiers in Materials 7, p. 56. ISSN: 2296-8016. DOI: 10.3389/fmats.2020.00056. (Visited on 10/24/2023).

Wang, Zhe, Shuheng Huang, Guanghua Wen, Wenbo Jiang, Fuhang Chen, and Ping Tang (2020a). “Effects of Temperature on the Thermal Conductivity of Amorphous $CaO–SiO_2–Al_2O_3$ Slags: A Computational Insight”. In: Physical Chemistry Chemical Physics 22.16, pp. 8808–8816. DOI: 10.1039/D0CP00382D.

Wang, Zhe, Guanghua Wen, Qiang Liu, Shuheng Huang, Ping Tang, and Liang Yu (Mar. 2020b). “Estimating the Thermal Conductivity of $CaO–Al_2O_3–SiO_2$ Slags by Equilibrium Molecular Dynamics Simulations”. In: Journal of Non-Crystalline Solids 531, p. 119851. ISSN: 00223093. DOI: 10.1016/j.jnoncrysol.2019.119851. (Visited on 10/30/2023).

Waseda, Yoshio, Eiichiro Matsubara, and Kozo Shinoda (2011). X-Ray Diffraction Crystallography: Introduction, Examples and Solved Problems. Berlin, Heidelberg: Springer Berlin Heidelberg. ISBN: 978-3-642-16634-1 978-3-642-16635-8. DOI: 10.1007/978-3-642-16635-8. (Visited on 11/20/2023).

Yang, Ding, Hanghang Zhou, Jian Wang, Zhengde Pang, Guishang Pei, Zhiming Yan, Hongxia Mao, Guibao Qiu, and Xuewei Lv (May 2021). “Influence of TiO2 on Viscosity, Phase Composition and Structure of Chromium-Containing High-Titanium Blast Furnace Slag”. In: Journal of Materials Research and Technology 12, pp. 1615–1622. ISSN: 22387854. DOI: 10.1016/j.jmrt.2021.03.069. (Visited on 09/26/2023).

Zhang, Ling, Annelies Malfliet, Bart Blanpain, and Muxing Guo (Aug. 2021). “In Situ Electrical Conductivity Measurement by Using Confocal Scanning Laser Microscopy”. In: Metallurgical and Materials Transactions B 52.4, pp. 2563–2572. ISSN: 1073-5615, 1543-1916. DOI: 10.1007/s11663-021-02210-w. (Visited on 10/03/2023).

Zheng, Kai, Zuotai Zhang, Lili Liu, and Xidong Wang (Aug. 2014). “Investigation of the Viscosity and Structural Properties of CaO-SiO2-TiO2 Slags”. In: Metallurgical and Materials Transactions B 45.4, pp. 1389–1397. ISSN: 1073-5615, 1543-1916. DOI: 10.1007/s11663-014-0053-8. url: https://link.springer.com/10.1007/s11663-014-0053-8 (visited on 06/26/2023).

Stéfan Zaaiman

Research Scientist
Ex Mente Technologies

Stéfan Zaaiman is a Ph.D. student at the University of Pretoria in the Department of Chemistry. He completed his MSc in 2023 in the field of theoretical chemistry investigating water clusters from a molecular wide perspective. His Ph.D. field of study is in solution models with a focus on the thermophysical properties calculated from slag solution models. He has a scholarship at Ex Mente Technologies where he is a member of the material science team.